THERMAL HELIUM DESORPTION SPECTROMETRY OF HELIUM-IMPLANTED IRON–D. Xu, T. Bus, S. C. Glade, and B. D. Wirth (University of California, Berkeley)

OBJECTIVE

The objective of this work is to understand the kinetics and energetics of helium transport and clustering in iron implanted with He ions as a function of He ion energy and dose.

SUMMARY

Elemental iron implanted with He at different energies and doses is studied using thermal helium desorption spectrometry (THDS). Currently examined energies and doses include: 100 keV, and 1 x 10^{11}, 1 x 10^{13}, and 1 x 10^{15} He/cm^2, respectively. While no clear desorption signals have been observed for the two lower dose samples, the present results reveal that for the iron implanted to 1 x 10^{15} He/cm^2 the majority of the implanted He atoms desorb at ~ 1000ºC and at > 1100ºC. Both conventional reaction model and Johnson-Mehl-Avrami (JMA) transformation model kinetics were utilized to fit the lower temperature (~ 1000ºC) desorption event of the 1 x 10^{15} He/cm^2 dosed iron. Surprisingly, single (either 1st or higher) order fits can not adequately describe the event. Excellent fits are obtained when combining a lower (n ~ 1.1) order with a higher (n ~ 5.8) order JMA fit. Additionally, spurious desorption peaks and certain complex desorption features have been observed which may affect future THDS studies.

PROGRESS AND STATUS

Introduction

The development of fusion reactors requires knowledge of material behavior under fusion environments, in particular with regard to high levels of helium produced by (n,α) reactions. It has been established that implanted or internally produced He can cause significant mechanical property degradation [1-5]. A crucial aspect, therefore, is to understand how helium atoms migrate and are trapped by microstructural features in irradiated materials. While a large amount of theory, modeling and experimental research has been performed in the past years, the understanding of this problem is still far from complete. Thermal helium desorption spectrometry (THDS) has been employed to experimentally study irradiation-induced structural defects and their interactions with He atoms in a variety of materials. For example, nucleation and growth of He-vacancy clusters were reported in vanadium and vanadium alloys [6], and the sequential releases of interstitial He and He-Vacancy clusters were reported in SiC [7] based on the THDS spectra.

In iron and ferritic alloys, computer simulations have been performed on defect production in collision cascades caused by helium injection [8], effect of He-vacancy complexes on the mechanical properties [9], thermal stability of He-vacancy clusters in iron [10], and the He-grain boundary interaction [11]. Experimentally, nuclear reaction depth profiling [12], transmission electron microscopy [13], positron annihilation lifetime and coincidence Doppler broadening (CDB) techniques [14,15] have been used in addition to THDS [10,16–17] to study the He migration and He-induced defect clusters in iron.

In this work, we use THDS to study the kinetics and energetics of helium in iron implanted with 100 keV He to three different doses, 1 x 10^{11}, 1 x 10^{13}, and 1 x 10^{15} He/cm^2. Constant rate heating ramps were employed to thermally desorb the implanted He. The resulting desorption signals were fit to both conventional reaction model and Johnson-Mehl-Avrami (JMA) transformation model kinetics. Surprisingly, single (either 1st or higher) order fits can not adequately describe the signals in either model. Excellent fits were obtained when combining a lower (~ 1) order with a higher (~ 6) order in the JMA model. Spurious desorption peaks and complex desorption features observed are also presented.

Experimental Methods

Figure 1 is a sketch of our recently built THDS at UC Berkeley [18]. Both the sample chamber and the measurement (quadrupole mass spectrometer) chamber are maintained at ultra-high vacuum with a pressure of about 10^{-10} Torr (at room temperature). Both the sample holder and the resistive heating filament are made of tungsten. The He, as well as other species (N_2, H_2, etc.), is signaled by the mass spectrometer (maintained at room temperature) while the sample is being heated according to a desired temperature profile. The synchronized sample heating and mass spectrometer measurement are both controlled through a LABVIEW program which simultaneously records all relevant data. During an actual measurement, liquid N_2 is constantly flowing through a channel between the inner and outer walls of the sample chamber to prevent the temperature rise of the walls and subsequent heating of the gas species.

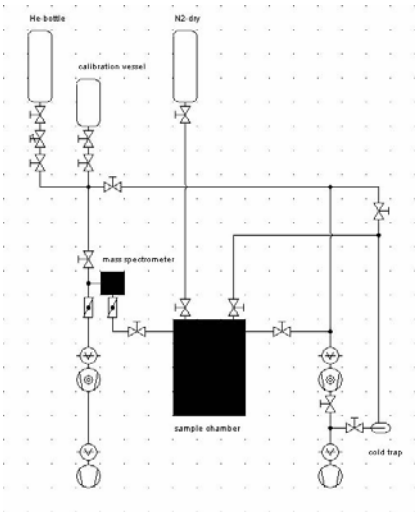

Fig. 1. Structural sketch of the Berkeley THDS instrument.

A THDS system can be operated in either static (no pumping during a measurement) or dynamic mode (gas being constantly pumped out during a measurement). In this study, dynamic mode was employed to prevent accumulation of desorbed He in the measurement chamber. In the dynamic mode with a fixed chamber volume *V*, assuming He at room temperature T_r, the He pressure inside the chamber *P*, as seen by the mass spectrometer, is governed by the differential equation:

$$VdP = K_B T_r d\overline{N} - \frac{PV}{\tau} dt \,, \tag{1}$$

in which τ is a pumping time constant, and $d\overline{N}$ is the number of desorbed He atoms from the sample in the time period of *dt*. The pumping constant τ is determined by the pumping speed and thus is adjustable. If τ is very small such that $dP/dt << P/\tau$ [1], then one obtains $d\overline{N}/dt \propto P$. However, as will be shown and discussed later, even when τ is indeed negligible, some non-negligible spurious signals (even peaks) which apparently do not result from the desorption of implanted He may still contribute to the measured pressure *P*. Therefore, a more careful expression should be: $d\overline{N}/dt \propto (P - P_{base})$ where P_{base} can be regarded as the signal measured from an otherwise-similar but non-implanted control sample. The control measurements were performed using the same settings (including the temperature control parameters,

[1]The accuracy of this assumption can be checked during data analysis by numerically comparing these two terms. τ can be found in calibration procedure. In this work, τ = 0.3s and the assumption is sufficiently satisfied.

the starting system pressure, the liquid N_2 flow rate, etc.) as for the corresponding actual desorption measurements.

A tube of 1 ml volume in connection with a 500 ml reservoir was used for calibration measurements. The calibration factor for the mass spectrometer was determined to be ~ 5.5 x 10^{-22}C/He-atom. Iron plates of 1mm thickness with a purity of 99.5% were purchased from Goodfellow and then commercially implanted with 100 keV helium to three different doses: 1 x 10^{11}, 1 x 10^{13}, and 1 x 10^{15} He/cm^2. Constant rate heating ramps at rates of 0.5 K/s and 1 K/s were used for both the control and the actual desorption measurements.

Results and Discussion

TRIM/SRIM calculations

The damage, He distribution, V/He (Vacancy/He) ratio and other factors related to He implantation in Fe were calculated with TRIM (SRIM 2003) software [19]. For 100 keV He implantation, the vacancy/He ratio is 87 and the peak He concentration at a dose of 1 x 10^{15}/cm^2 is about 700 appm, which appears at a depth of 340 nm.

Spurious peaks

A comparison between two samples: S10 (1 x 10^{15}/cm^2 dosed) and S12 (non-implanted control) is shown in Fig. 2a. The same heating control parameters were used for both samples which produced almost identical actual temperature profiles during the measurements. Fig. 2a shows that both samples exhibit a set of medium temperature He peaks in the range of ~ 600–880ºC, and, more importantly, the positions of these medium temperature peaks are almost identical for the two samples. However, the implanted sample S10 displays much stronger signals than the non-implanted S12 at temperatures higher than ~ 880ºC, including a fully developed peak at 1017ºC and a broad peak with an onset of ~ 1130ºC.

Apparently, the medium temperature peaks in the range of ~ 600–880ºC are not due to the desorption of implanted He, and thus are referred to as spurious peaks (signals) throughout this paper. The real identifiable desorption events start from above 880ºC in the 1 K/s ramping measurement of S10. Since the magnitudes of the spurious peaks are not negligible compared with the real desorption peaks, it is thus crucial to perform a control analysis before making peak assignments, particularly if the He desorption under consideration occurs in a relatively low temperature range (e.g., below 880ºC). Whether such spurious peaks also contributed to the observed signals in previous THDS studies is unclear.

While the exact origin of the spurious peaks is still under investigation, they appear to be related to the mutual desorption of several non-implanted species. As shown in Fig. 2b, other channels of the mass spectrometer, such as N_2, as well as the total system pressure, also exhibit peaks at basically the same temperatures.[2] Moreover, even a copper gasket was found to exhibit similar peaks on all channels of the mass spectrometer (including He) at relatively lower temperatures from 500 to 750ºC. It must also be noted that these spurious peaks do not appear when an empty-chamber (without any sample) is measured, indicating system cleanliness is not the problem. Rather it appears that surface contamination of the sample might be partly responsible for the spurious peaks.

[2]These other channels are distinguished from the He channel at temperatures higher than ~ 880 ºC where the implanted He starts to desorb. Note that a logarithm scale is used in Fig. 2b for comparison of different channels.

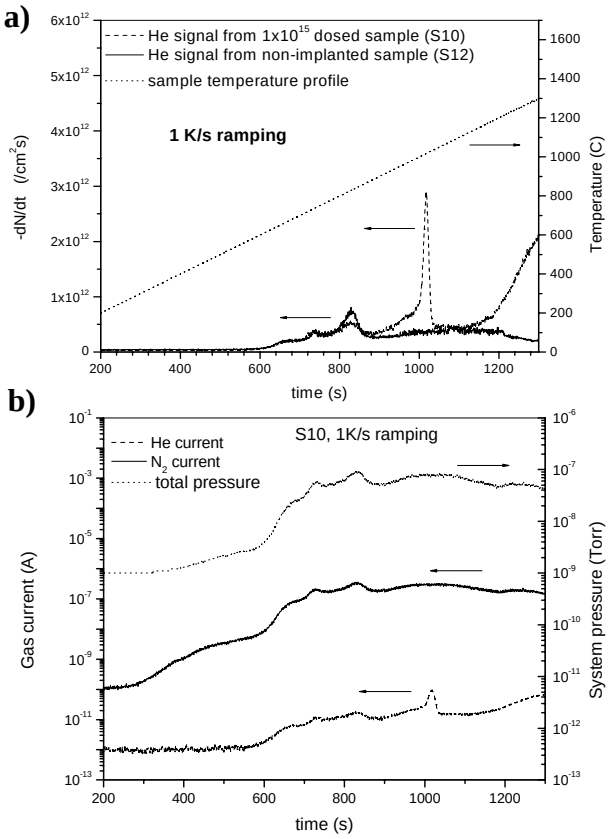

Fig. 2. a) Comparison between He signals measured from two samples, S10 (1 x 10^{15}/cm^2 dosed) and S12 (non-implanted); and b) correlations among He signal, other gas signals (represented by N_2), and total system pressure, measured from sample S10—note that a logarithmic scale is used.

Samples of 1 x 10^{15}/cm^2 dose

- *Reaction model analysis*

From the 1 K/s (β_1) constant rate ramping data presented in Fig. 2a (dashed line), the peak temperature T_p of the first desorption event of the 1 x 10^{15}/cm^2 dosed iron was determined to be 1017ºC. The ramping measurement was also performed at a heating rate of 0.5 K/s (β_2), which shifted the T_p to 993ºC.

A number of previous studies (e.g., [20]) have assumed that He desorption obeys a 1st order chemical reaction model, i.e., $dN/dt = -K_0 \exp(-Q/K_B T) * N$, where N is the number of remaining He atoms in the sample corresponding to a given desorption event, K_0 is a frequency factor, Q is the activation energy of the desorption event, and K_B is the Boltzmann constant. By solving the equation $d^2N/dt^2 = 0$ under the constant rate ramping condition (i.e., $dT/dt = \beta$), it can be found that the peak temperature T_p on the dN/dt signal satisfies the equation $\ln(\beta/T_p^{\,2}) = -Q/K_B T_p + \ln(K_0 K_B/Q)$. Therefore, the use of two

sets of T_p vs. β data can determine both the activation energy Q and the frequency factor K_0. In this case, we obtain $Q = 3.8$ eV and $K_0 = 2.04 \times 10^{13}$ /s. Nevertheless, as shown in Fig. 3, a back-calculation of dN/dt using these parameters and the assumed 1st-order reaction model reveals that the 1st order assumption in fact does not provide satisfactory agreement with the experimental peak, particularly with respect to the peak sharpness (half-maximum width) and steepness. Moreover, even when Q and K_0 are allowed to vary around these values (3.8 eV and 2.04×10^{13} /s), similar fit curves are obtained and the sharpness of the entire event still can not be adequately described.

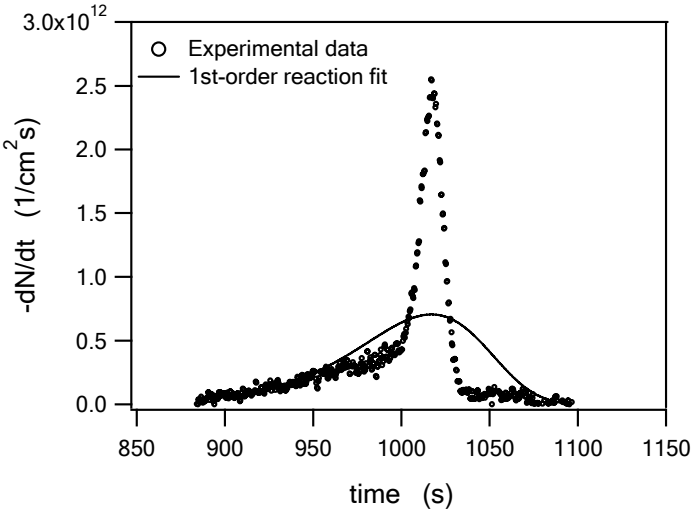

Fig. 3. First-order fit using reaction model for the 1017ºC desorption event of the 1 x 10^{15}/cm^2 dosed sample: $n = 1$, $Q = 3.81$ eV, $K_0 = 2.04 \times 10^{13}$ /s.

- *Johnson-Mehl-Avrami (JMA) model analysis*

A non-1st-order reaction model was then considered in an attempt to obtain better fits. From the general form of the reaction model, i.e., $dN/dt = -K_0 \exp(-Q/K_B T) * N^n$ (where n is the order of reaction), one can obtain: $d^2N/dt^2 = dN/dt * [\beta Q/(K_B T^2) + (n/N) * dN/dt]$. Therefore, at the desorption peak, we have $Q/n = -[K_B T_p^2/(\beta * N_p)] * \left.\frac{dN}{dt}\right|_p$. N_p (as well, it is important to note that N is a function of t) can be numerically determined using the dN/dt data. Hence, Q/n is determined to be 15.8 eV for the 1017ºC desorption event. Thus we obtain $dN/dt = -K_0[N * \exp(-15.8/K_B T)]^n$. Hence, if the general form of the reaction model is a good description of the event, the plot of $\ln(-dN/dt)$ vs. $\ln[N * \exp(-15.8/K_B T)]$ should be close to a straight line with a slope of n and an intercept of $\ln K_0$. However, a plot of the 1017ºC event obeys this linearity only at the early stage (up to 1000 s, i.e., 1000 ºC) of the event, but significantly deviates thereafter, indicating the inadequacy of this general reaction model for the description of this event.

A JMA kinetic model [21,22] was then employed to analyze the desorption event at $T_p = 1017$ºC. The general form of the JMA model can be written as: $x = 1 - \exp(-K^n t^n)$, where $K = K_0 \exp(-Q/K_B T)$, x is the transformed (in this case, desorbed) fraction of He atoms corresponding

to a certain event, i.e., $x \equiv 1 - N(t)/N_0$. Therefore, the desorption rate can be derived as: $dN/dt = -N_0 dx/dt = -N_0 * nK^n t^{n-1} \exp(-K^n t^n) * [1 + \beta t Q/(K_B T^2)]$. According to Henderson's analysis (Appendix A7 in Ref. [23]), the activation energy Q in this model[3] can be approximated using the peak shifting approach, i.e., $Q \approx$ slope of the plot of $\ln(\beta/T_p^{\,2})$ vs. $-1/K_B T_p$ [4]. Analysis of the two sets of T_p vs. β data presented earlier results in $Q \approx 3.8$ eV. Thus, we fixed Q to this value and varied n and K_0 to obtain a series of fits for the desorption signal, four of which are shown in Fig. 4. As was the case with the 1st-order-reaction fit, the 1st-order JMA fit can not describe the sharpness of the desorption peak. However, as the order n increases, the JMA fit gets finer and the fit-peak increases such that it better accounts for the sharpness of the experimental peak. On the other hand, a higher order (e.g., $n = 4$) JMA fit can not adequately describe the early stage ($t < 1000$ s) of the experimental signal.

The fact that neither the 1st order, nor a single higher order fit can satisfactorily account for the entire signal leads to the hypothesis that more than one single-order event is involved. Indeed, as shown in Fig. 5, by combining a low order component with a high order component within the JMA model, the entire signal can be fit very well. The fitting methodology is described in the Appendix. The fit result suggests that ~ 44% of the total He atoms involved in this entire event desorb according to a low order (n ~ 1.1) in the early stage and the remaining 56% desorb with a higher order (n ~ 5.8). However, the microscopic mechanism underlying this order change during a single desorption event requires further investigation.

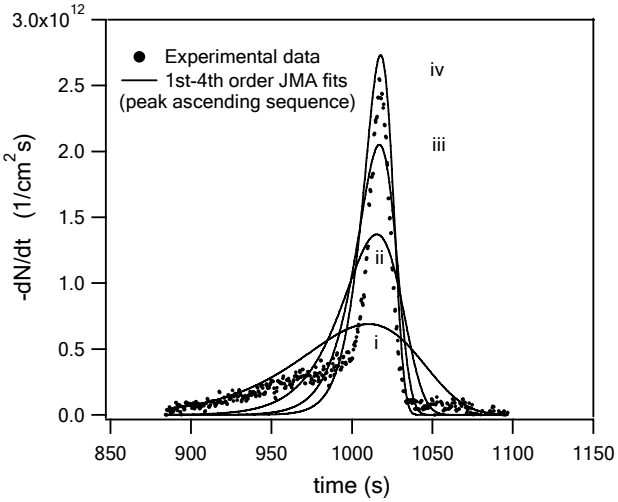

Fig. 4. Single-order JMA fits for the 1017ºC desorption event of the 1 x 10^{15}/cm^2 dosed sample, with fixed activation energy $Q = 3.81$ eV, and varied n and K_0 (in the peak ascending sequence): a) $n = 1$ and $K_0 = 8.6 \times 10^{11}$ /s; b) $n = 2$ and $K_0 = 7.8 \times 10^{11}$ /s; c) $n = 3$ and $K_0 = 7.5 \times 10^{11}$ /s; d) $n = 4$ and $K_0 = 7.4 \times 10^{11}$ /s.

[3]Note that Q here is equivalent to the $\Delta H/n$ in Henderson's analysis, and K_0 here is equivalent to Henderson's $K_0^{1/n}$. The form used here is more reasonable in terms of physical meaning of the JMA model.

[4]This is essentially the same technique used for the determination of the activation energy in the earlier 1st-order reaction analysis. However, the intercepts in the two analyses are different.

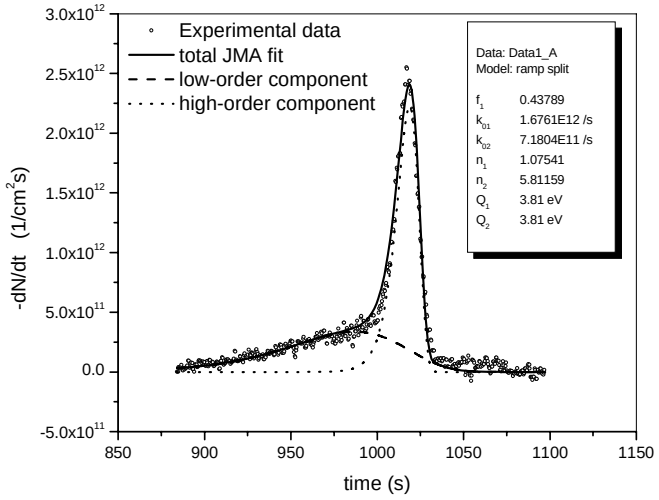

Fig. 5. Combined JMA fit for the 1017ºC desorption event of the 1 x 10^{15}/cm^2 dosed sample, consisting of a low order and a high order component. Note f_1 is the number fraction corresponding to the low order component (refer to the Appendix for fitting methodology).

Complex desorption behavior

The above analyses are based on the desorption signal recorded during the first heating ramp of a sample. However, this event was also observed during immediate cooling after first heating and even during subsequent (without opening chamber) re-heating and re-cooling, as illustrated in Fig. 6 by sample S3. Only after a sample was held isothermally at a very high (1330ºC) temperature for a long time (~ 30 min) did the event disappear completely during subsequent heat-up and cool down. While the existence of multiple de-trapping and migration mechanisms with a range of activation-energies is a tentative explanation for this complex behavior, the exact reason is not yet clear.

Samples of 1 x 10^{13} and 1 x 10^{11}/cm^2 dose

The ~ 1000ºC desorption event observed for the samples implanted to a He dose of 1x10^{15}/cm^2 was not unambiguously observed from the 1 x 10^{11} and 1 x 10^{13} He/cm^2 dosed samples for the same heating ramp conditions. Rather, these lower dosed samples exhibited very similar signals (spurious peaks) as the non-implanted samples. The absence of strong desorption signals from these two samples may not be a surprise since the total number of implanted He atoms in these samples is much lower than the 1 x 10^{15} He/cm^2 dosed sample. It appears necessary to improve the signal to noise ratio of the mass spectrometer in order to successfully detect any desorption events occurring in these lower dosed samples, in addition to performing the implantations at lower He ion energy.

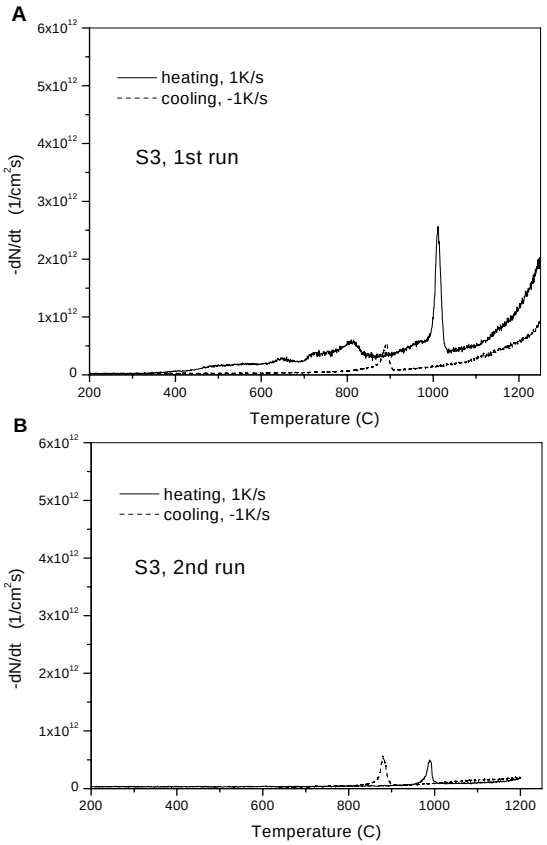

Fig. 6. First and second heating-cooling cycles of sample S3 showing the repetitive appearance of the same desorption event.

Conclusions

He desorption from iron implanted with 100 keV He to a dose of 1 x 10^{15}He/cm^2 occurs mainly at high temperatures (above 880ºC). Two desorption events have been observed for this sample during a constant rate ramping process: one with a fully developed peak at 1017ºC (in a 1 K/s ramp), the other with an onset of ~ 1100ºC, but not fully developed up to 1330ºC. The 1017ºC desorption event has been analyzed using both conventional reaction model and JMA model kinetics. First order equations from either model can only describe the broad early part of the event but not the steep desorption peak. A higher order JMA model can account for the peak steepness, but does not satisfactorily describe the early broad part. The superposition of a low-order (n ~ 1.1) and a high-order (n ~ 5.8) component produces excellent fits to the entire desorption event. The activation energy, Q, for this event was determined to be ~ 3.8 eV based on the peak shift with heating rates, and was confirmed by the data fitting. He desorption signals from the 1 x 10^{11} and 1 x 10^{13}/cm^2 He implanted samples have not been successfully detected at present. Future efforts will focus on a systematic examination of He release as a function of implanted He ion energy and dose, in addition to further analysis to determine the governing He de-trapping and migration mechanisms controlling the release peaks at 1017 and ~ 1100ºC.

Acknowledgements

This work has been supported by the Office of Fusion Energy Sciences, U.S. Department of Energy, under Grant DE-FG02-04ER54750.

Appendix

Methodology for the two-order JMA fit (shown in Fig. 6) for the 1017ºC desorption event of the 1 x 10^{15} /cm^2 dosed sample:

1) $N_{01} = f_1 * N_0$ and $N_{02} = (1 - f_1) * N_0$;
2) $dN / dt = dN_1 / dt + dN_2 / dt$;
3) $dN_i / dt = -N_{0i} * dx_i / dt = -N_{0i} * n_i K_i^{n_i} t^{n_i - 1} \exp(-K_i^{n_i} t^{n_i}) * [1 + \beta * tQ_i / (K_B T^2)]$ $(i = 1,2)$;
4) $K_i = K_{0i} \exp(-Q_i / K_B T)$ $(i = 1,2)$,

where f_1 is the number fraction corresponding to the low order component, and N_0 is the total number of He atoms for the entire desorption event.

References

[1] E. E. Bloom and F. W. Wiffen, J. Nucl. Mater. 58 (1975) 171.
[2] L. K. Mansur and W. A. Coghlan, J. Nucl. Mater. 119 (1983) 1.
[3] H. Ullmaier, Nucl. Fusion 24 (1984) 1039.
[4] L. K. Mansur and M. L. Grossbeck, J. Nucl. Mater. 155 (1988) 130.
[5] H. Trinkaus and B. N. Singh, J. Nucl. Mater. 323 (2003) 229.
[6] A. V. Fedorov, A. van Veen, and A. I. Ryazanov, J. Nucl. Mater. 233 (1996) 385.
[7] E. Oliviero, M. F. Beaufort, J. F. Barbot, A. van Veen, and A. V. Fedorov, J. Appl. Phys. 93 (2003) 231.
[8] I. Mori, T. Morimoto, R. Kawakami, and K. Tominaga, Nucl. Instrum. Methods Phys. Res. B 153 (1999) 126.
[9] A. A. Selezenev, V. G. Golubev, and N. S. Ganchuk, Chem. Phys. Rep. 17 (1998) 295.
[10] K. Morishita, R. Sugano, B. D. Wirth, and T. D. de la Rubia, Nucl. Instrum. Methods Phys. Res. B 202 (2003) 76.
[11] R. J. Kurtz and H. L. Heinisch, J. Nucl. Mater. 329 (2004) 1199.
[12] M. B. Lewis and K. Farrell, Nucl. Instrum. Methods Phys. Res. B 16 (1986) 163.
[13] K. Arakawa, R. Imamura, K. Ohota, and K. Ono, J. Appl. Phys. 89 (2001) 4752.
[14] T. Ishizaki, Q. Xu, T. Yoshiie, and S. Nagata, Mater. Trans. 45 (2004) 9.
[15] T. Iwai, Y. Ito, and M. Koshimizu, J. Nucl. Mater. 329 (2004) 963.
[16] R. Sugano, K. Morishita, A. Kimura, H. Iwakiri, and N. Yoshida, J. Nucl. Mater. 329 (2004) 942.
[17] R. Vassen, H. Trinkaus, and P. Jung, Phys. Rev. B 44 (1991) 4206.
[18] S. C. Glade, B. D. Wirth, and H. Schut, Fusion Materials Semiannual Progress Reports, DOE/ER-0313/37 (2004) 136.
[19] J. F. Ziegler, J. P. Biersack, and U. Littmark, The Stopping and Range of Ions in Matter, Pergamon, New York (1984).
[20] A. van Veen, A. Warnaar, and L. M. Caspers, Vacuum 30 (1980) 109.
[21] W. A. Johnson and R. F. Mehl, Trans. Am. Inst. Min. Metall. Engs. 135 (1939) 416.
[22] M. Avrami, J. Chem. Phys. 7 (1939) 1103.
[23] D. W. Henderson, J. Non-Cryst. Solids 30 (1979) 301.